SAC/EPSA/OCEANSAT-3/ATBD/OP-02/OCT-2021-V1

Algorithm theoretical basis document (ATBD) for Geophysical parameter retrieval using EOS-6 (OCEANSAT-3) OCM

March

2023

Space Applications Centre

Indian Space Research Organization

Government of India

Ahmedabad-380015

DOCUMENT CONTROL AND DATA SHEET

1.	Date	March 2023
2.	Title	Algorithm theoretical basis document (ATBD) for Geophysical parameter retrieval using EOS-6 (OCEANSAT-3) OCM
3.	Doc. No.	SAC/EPSA/OCEANSAT-3/ATBD/OP-02/OCT-2021-V1
4.	Type of Report	Technical - Algorithm Theoretical Basis Document (ATBD)
5.	No. of Pages	35
6.	Authors	Anurag Gupta, Debojyoti Ganguly, Arvind Sahay, T. Devi Prasad, P.V. Nagamani, Mini Raman
7.	Originating Centre	Space Applications Centre (ISRO), Ahmedabad
8.	Abstract	The objective of EOS-6 Ocean Colour Monitor (OCM-3) is to carry forward the legacy of OCEANSAT: OCM-1 and 2 by providing the quantitative information on bio-optical constituents such as chlorophyll-a concentration, vertical diffuse attenuation coefficient of light (Kd) at 490nm, concentration of total suspended matter in coastal waters etc. to the user community. The Algorithm Theoretical Basis Document (ATBD) describes the atmospheric correction technique with other bio-optical models for generating the operational products - water leaving radiance/remote sensing reflectance, aerosol optical thickness at 870nm, chlorophyll-a concentration, vertical diffuse attenuation coefficient at 490nm and total suspended matter (TSM) using EOS-6 OCM data.
9.	Keywords	Atmospheric correction, Remote sensing reflectance, Chlorophyll-a, Kd, TSM, aerosol optical thickness at 870nm
10.	Approving Authority	Oceansat-3 ATBD Review Committee
11.	Classification	Unrestricted
12.	Circulation	Open

Algorithm theoretical basis document (ATBD) for Geophysical parameter retrieval using EOS-6 (OCEANSAT-3) OCM

1.0 Algorithm Specifications:

Version	Date	Prepared by	Description
1.1	29/03/2023	Anurag Gupta, Debojyoti Ganguly, Arvind Sahay, T. Devi Prasad, P.V. Nagamani, Mini Raman	Retrieval of remote sensing reflectances and bio-optical parameters - *Chl-a*, K_d (490) and TSM from EO-6 OCM3.

2.0 Introduction

Satellite ocean-colour observations are now widely recognized as an important component of international remote sensing programs. Chlorophyll, the primary product of ocean-colour sensors, is a measure of marine phytoplankton biomass. Phytoplankton are responsible for approximately half the global photosynthetic uptake of carbon (Field *et al*., 1998). In response to the potential importance of phytoplankton in the global carbon cycle and the lack of comprehensive data, the international community has established high priority satellite missions designed to acquire and produce high quality global ocean-colour data. One of the goals of launching a number of ocean-colour sensors aboard various satellites is to build a long-term, multi-sensor, multi-year, ocean-colour archive (IOCCG, 1999; McClain, 1998). The derived chlorophyll concentrations (in time and space) can be used to resolve inter-annual-to-decadal changes in oceanic phytoplankton biomass in response to global environmental changes. Ocean colour remote sensing deals with quantitative estimation of the bio-optical properties from space borne measurements. VIS-NIR region pertaining to the electromagnetic spectrum, is of prime concern to study the subsurface water column. The light interactions with optical constituents in the water column take place significantly in terms of multiple scattering and absorption and as a

consequence, the resultant signal from water column reaches the sensor in space. Thus, the remote sensing reflectance is derived by removing the absorption and scattering due to gaseous molecules and particles present in the atmosphere from TOA radiance, followed by retrieval of bio-optical constituents using well known bio-optical algorithms.

The objective of EOS-6 Ocean Colour Monitor (OCM-3) is to carry forward the legacy of OCEANSAT – OCM-1 and 2 by providing the quantitative information on bio-optical constituents such as chlorophyll-a concentration, vertical diffuse attenuation coefficient of light (Kd) at 490nm, concentration of total suspended matter in coastal waters etc. to the user community. The Algorithm Theoretical Basis Document (ATBD) describes the atmospheric correction technique with other bio-optical models for generating the operational products - water leaving radiance/remote sensing reflectance, aerosol optical thickness at 870nm, chlorophyll-a concentration, vertical diffuse attenuation coefficient at 490nm and total suspended matter (TSM) using EOS-6 OCM data.

2.1 OCEANSAT-3 OCM Instrument

Ocean Colour Monitor (OCM)-3 on board EOS -6 is designed to measure spectral variation of water leaving radiances that can be related to phytoplankton pigment concentration, total suspended matter and coloured dissolved organic matter in ocean waters, as well as aerosol characterization in the atmosphere. It is envisaged to provide service continuity for the operational users of OCM data from OCEANSAT-2. OCM-3 has 13 bands in VNIR (400-1010 nm range) with 1440 km swath for ocean colour monitoring. OCM-3 will be operated in two modes such as a) Local Area Coverage (LAC) mode, to cater mainly for user's real-time requirement of high resolution data (360 m). b) Global Area Coverage (GAC) mode, to cover the global ocean at regular cycles in low resolution mode (1 km). The spectral bands, associated central wavelengths, their bandwidths and potential applications are given in Table 1. The details of technical characteristics of the sensor are provided in Table 2 & 3.

Band No	OCM-III		Potential Applications
	Central wavelength (nm)	Bandwidth (nm)	
1	412	20	Yellow substance absorption
2	443	10	Low Chlorophyll-a concentration
3	490	10	Medium Chlorophyll-a concentration, diffuse attenuation coefficient
4	510	10	High Chlorophyll-a concentration
5	555	10	Chlorophyll-a reference, turbidity
6	566	10	Trichodesmium identification
7	620	10	Suspended sediments, cyanobacteria, Turbidity in case-2 waters
8	670	10	Baseline for chlorophyll fluorescence
9	681	08	Chlorophyll fluorescence
10	710	10	Baseline for chlorophyll fluorescence, red edge
11	780	10	Atmospheric correction
12	870	20	Atmospheric correction, spectral scattering
13	1010	20	Atmospheric correction for turbid waters, aerosol – white foam discrimination

Table 1: Central wavelengths, bandwidth and application potential of E0S-6 OCM-3.

Parameter	Value
IGFOV (m)	366
Total lens assemblies and DHA	13
Pixel size and pitch (μm)	10
Detector format (pixels)	4000 x 48
Focal length (mm)	20
F-number	4.3/4.5
Field-of-view (°)	±43.5
Integration time	53.46 ms
Transmission bits	12/16
SNR at reference radiance	> 1000 for B1 to B10 > 800 for B11 to B13

Table 2: *OCM-3* Sensor Specifications

Bands	Band definition (nm)	Transmission bits	Ocean reference radiance (mw/cm^2/sr/um)	Saturation radiance (mw/cm^2/sr/um)	SNR at Ocean reference
B1	407-417	12 bits (LAC) 16 bits (GAC)	9.1	100% albedo	>1000
B2	438-448		8.4		>1000
B3	485-495		6.6		>1000
B4	505-515		5.6		>1000
B5	550-560		4.6		>1000
B6	561-571		4.3		>1000
B7	615-625		3.1		>1000
B8	665-675		2.5		>1000

B9	677-685	12	2.3		>1000
B10	705-715		2.0		>1000
B11	775-785		1.6		>800 (1080m)
B12	860-880		1.1		>800 (1080m)
B13	1000-1020		0.5		>800 (1080m)

Table 3: Baseline design goals of OCM-3: Radiometric parameters

3.0 Overview & background

3.1 Theoretical background

Estimation of water-leaving radiance from TOA radiance involves removing contribution of atmospheric-path radiance and surface reflected radiance from the measured signal. Atmospheric correction technique first applied for satellite imagery of ocean color was developed by Gordon (1980). This technique was based on the assumption that Rayleigh and aerosol scattering is separate and contribution to total measured radiance by both the processes were calculated independently. In this process, radiance directly reflected from the surface (known as specular reflection) was ignored and the ocean surface was assumed flat. Initial calculation of Rayleigh scattering based on single scattering approximation had significantly large errors for higher solar zenith angle. To reduce such errors, Gordon et al., 1988 developed a fast and accurate scheme for Rayleigh scattering using vector radiative transfer code (which included polarization effect). These computations when applied to CZCS imagery gave accurate atmospheric correction up to a solar zenith angle of 65 degrees. Another important source of error in retrieving water leaving radiance is introduced from the single scattering approximation, where the scattering from aerosol and gas molecules are assumed to be independent. Deschamps et al. (1983) showed that for instruments with higher radiometric sensitivity, such an assumption leads to significant errors in the retrieval of water leaving radiance. Gordon and Wang (1994a) developed a detailed atmospheric correction algorithm for sensors with higher

radiometric sensitivity such as SeaWiFS/ MODIS which included accurate calculations of Rayleigh scattering and the multiple scattering effects of aerosol and gas molecules. Gordon and Wang (1994a) have shown that the multiple scattering in atmosphere depends significantly on the type of aerosol model used. To account for such effect, 12 aerosol models have been used in the processing of SeaWiFS/MODIS data sets (Gordon and Wang, 1994a; Wang *et al.*, 2005). Information on aerosol model and aerosol optical depth over the ocean is derived from near Infrared (NIR) channels, since the oceanic signal is assumed to be zero in this part of the spectrum (black pixel approximation). This assumption yields good result in Case I open ocean waters, but when applied to turbid coastal or Case II waters the algorithm frequently results in negative values of water leaving radiance. This is due to the fact that constituents in coastal case II waters are mainly dominated by suspended sediments, which can contribute significantly to water leaving radiance in NIR bands.

Atmospheric correction of hyperspectral data using radiative transfer code was first proposed by Gao et al. (2009) where the scattering from atmospheric aerosols and molecules were computed using 5S computer code. This information along with the solar and viewing geometry were used to generate transmission spectra of various atmospheric gases such as H_2O, CO_2, CO, O_3, O_2 etc. with the help of narrow band spectral model. Atmospheric correction of top of the atmosphere radiance requires very accurate modeling of scattering and absorption effects in the atmosphere. This is mainly due to the fact that the signal leaving the water surface is weak. Many other works (Gao et al. 2000, 2007, 2009) demonstrated to correct for atmospheric effects.

3.2 Global Scenario

Satellite based ocean-colour measurement has emerged as one of the important area of gathering information on bio-geo-chemical variability of oceans on a global and regional scale. The launch of Nimbus-7 satellite in 1978 carrying Coastal Zone Colour Scanner (CZCS) heralded a new era in field of biological oceanography. The demise of CZCS in 1986 left a decade-long void in the continuity of ocean colour data from space. Subsequently, in mid-1990's three satellites were launched. MOS (Modular Optoelectronic Scanner), by the German Aerospace Agency (DLR) on-board IRS-P3 satellite, Ocean Colour and Temperature Sensor (OCTS) on-board Advanced Earth Observation Satellite (ADEOS) by Japan and SeaWiFS (Sea Viewing Wide Field-of-View

Sensor) on-board OrbView2 by NASA. The SeaWiFS local area coverage (LAC) at 1 km spatial resolution and global area coverage at 9 km spatial resolution data has been extensively used worldwide for numerous applications in ocean biology. Currently data from a number of ocean colour sensors launched by Japan, U.S.A, Korea, China and Europe are available to the user community for global and regional studies. Foremost among these are two MODIS sensors (Moderate Resolution Imaging Spectroradiometer) launched by NASA on the TERRA and AQUA, VIIRS (Visible Infrared Imager Radiometer Suite) on SUOMI–NPP and JPSS, MERIS (Medium Resolution Imaging Spectrometer), OLCI (Ocean Land Color Instrument) on Sentinel 3 A & 3B by ESA. Korea launched two Geostationary Ocean Colour Imager (GOCI -1 and GOCI-II). There are 4 Chinese ocean colour sensors currently providing the data which are Chinese Ocean Colour and Temperature Scanner (COCTS) with a spatial resolution of 1.1 km, Coastal Zone Imager (CZI) with a spatial resolution of 250m and 2 Medium Resolution Spectral Imager (MERSI) onboard FY-3A and FY-3B. Second-Generation Global Imager (SGLI) on Global Change Observation Mission-C (GCOM-C) was launched by Japan in 2017. Technique for atmospheric correction are based on radiative transfer equations, which describe the interactions between the various atmospheric constituents and sea surface affecting the satellite measurements. For ocean colour sensors having bands limited to NIR region, standard atmospheric correction procedure involving radiative transfer equations are applied to retrieve remote sensing reflectances. The classical 'black pixel' approach assumes negligible water radiance in NIR bands and determine independently the aerosol radiance at 765 and 865 nm. The SeaWiFS algorithm of Gordon and Wang (1994) computes the radiative transfer in the ocean-atmosphere system for a reference set of aerosol models. Multiple scattering is fully accounted for in this algorithm, but the algorithm relies strongly on the choice of aerosol models. Fukushima *et al*. (2000) also developed an atmospheric correction algorithm for analysis of OCTS data using multiple scattering and aerosol model based approach, almost similar to the one used for SeaWiFS processing. Standard atmospheric correction algorithms fail over turbid coastal waters as the assumption about zero water-leaving radiance in NIR region of electromagnetic spectrum fails due to high backscattering of suspended sediment and other inorganic particulates (Mao *et al*. 2013). The non-zero water-leaving radiance in near-infrared results in an overestimation of the aerosol optical thickness in blue-green regions of electromagnetic spectrum, leading to an atmospheric 'over-correction' in

the visible part of spectrum. As a result, negative water leaving radiances at shorter wavelengths are generated in coastal waters. Ruddick *et al,* (2000) developed a method which assumes spatial homogeneity of 765:865 nm ratios of aerosol as well as water-leaving radiance whereby a user must interactively determine an aerosol type. This method solves for aerosol radiance and water leaving radiance simultaneously in the NIR and was successfully applied to highly scattering waters of the North Sea. Bio-optical algorithms quantitatively relate variations in the concentration of bio-optical properties to ratios of radiance measurements at various wavelengths. The currently operational global ocean chlorophyll-a algorithm (Ocean Chlorophyll-4) is a cubic polynomial function based band switching algorithm that uses maximum remote-sensing reflectance ratio of 443, 490 and 510 nm to 555 nm band and has been developed based on an extensively calibrated and enhanced set of *in-situ* measurements.

3.3 Indian Scenario

India has a committed program on Ocean Colour. The first Ocean Colour Monitor (OCM) was launched on May 26, 1999 on board the Indian Remote Sensing Satellite Oceansat -1 IRS-P4) to collect valuable data set on the bio-optical parameters from space. Following the success of Oceansat-1 and to provide continuity of ocean-colour data, ISRO launched a second satellite Oceansat-2 on September 24, 2009 with OCM-II to further enhance the study of oceans. Data from OCEANSAT-1 OCM and Oceansat-2 OCM, has been operationally utilized for PFZ forecast by INCOIS. Apart from the operational use, data from OCM-1 and OCM2 has been utilized for various biological and geo-physical applications like studying coastal processes, aerosol radiative forcing, physical-biological coupled processes and primary and secondary productivity estimates, sea surface nitrate mapping, species specific fishery forecast etc. OCM-1 and OCM-2 comprised of eight spectral bands in the visible and near infrared (VNIR) region of electromagnetic spectrum to collect data on the objects of interest (targets) as well as for atmospheric correction. However, OCM-3 which is an improvement over OCM-1 and 2 will have more than eight spectral bands in the region of 0.407 to 1.020 microns to meet the advanced imaging requirements and application needs. Table 4 gives a glimpse of the enhancements in OCM-3 over OCM 1 and 2.

Table 4: Enhancements in OCM-3 over OCM-1 and 2

S.No	OCM-1	OCM-2	OCM-3
	B1 – 412 nm	B1 – 412 nm	B1 – 412 nm
	B2 – 443 nm	B2 – 443 nm	B2 – 443 nm
	B3 – 490 nm	B3 – 490 nm	B3 – 490 nm
	B4 – 510 nm	B4 – 510 nm	B4 – 510 nm
	B5 – 555 nm	B5 – 555 nm	B5 – 555 nm
	B6 – 640 nm	B6 – 620 nm	B6 – 566 nm
	B7 – 765 nm	B7 – 740 nm	B7 – 620 nm
	B8 – 865 nm	B8 – 865 nm	B8 – 670 nm
			B9 – 681 nm
			B10 – 710 nm
			B11 – 780 nm
			B12 – 870 nm
			B13 – 1010 nm
No. of bands	8 bands	8 bands	13 bands
SNR	300	300	1000
Bandwidth	20 nm (Application bands) 40 nm Atmos. Corr. bands	20 nm (Application bands) 40 nm Atmos. Corr. bands	10/8 nm (Application bands) 20 /40nm (Atmos. Corr. Bands)

Globally accepted standard atmospheric correction procedure to top-of-the–atmosphere radiances were adopted to retrieve remote sensing reflectances in OCM-1 & OCM-2 data. Black pixel approach in NIR bands and single scattering approximation was used to determine aerosol

radiance at NIR bands of OCM-1 and OCM-2. Bio-optical algorithms OC2 involving 490 and 555 nm bands and OC4 involving 4 bands 443, 490, 510 and 555 nm with regionally tuned coefficients were adopted for the retrieval of chlorophyll concentration. Regional datasets were used to empirically formulate algorithm for TSM. Through inter-sensor comparisons and extensive sea-truth collection campaigns, these algorithms were validated and have been shown to have the retrieval accuracies within the range defined for ocean colour missions.

4.0 Algorithm Description

4.1 Input Satellite Data (OCEANSAT-3 OCM data)

The algorithm uses band-averaged spectral radiance measured at the top of the atmosphere in each of the thirteen spectral bands of the OCM data along with the inputs on latitude, longitude, Julian day number, sun zenith, sun azimuth angles on a per pixel basis. The above inputs will be provided by the data products (DP) group of the Space Applications Centre, ISRO, Ahmedabad for operational processing.

Information on the spectral response functions (SRFs) of OCEANSAT-3 OCM sensor is required for the accurate calculation of band averaged extraterrestrial solar flux (F^0) by making use of extraterrestrial solar flux data of Thullier *et al. (2003).* The sensor specific SRFs is used for the calculation of band averaged Rayleigh optical depth and Ozone transmittance for all the thirteen bands of OCM-3 data.

$$\boldsymbol{F^0(\lambda)} = \int_{\boldsymbol{\lambda_1}}^{\boldsymbol{\lambda_2}} \frac{\boldsymbol{f(\lambda)g(\lambda)d\lambda}}{\boldsymbol{f(\lambda)}} \qquad (1)$$

Where $f(\lambda)$ is the spectral response functions (SRFs) of OCEANSAT-3 OCM sensor and $g(\lambda)$ is the extraterrestrial solar flux ranging from $\boldsymbol{\lambda_1}$ to $\boldsymbol{\lambda_2}$.

4.3 Development of Algorithm

The procedure adopted for retrieval of geophysical products depends on cloud free and glint free water pixels for daytime conditions over open ocean and coastal waters. Therefore, geophysical retrieval is performed only after land/cloud and sun glint mask for OCM-III top of the atmosphere radiance. After atmospheric correction, remote sensing reflectance/ normalized water leaving radiance over water is retrieved. Subsequently this output goes as an input to bio-optical

algorithms for the retrieval of chlorophyll concentrations (Chl-a), vertical diffuse attenuation coefficients K_d and total suspended matter (TSM).

4.3.1 Land masking

Oceanic information is extracted by masking land pixels from top of the atmosphere (TOA) radiance. The best way to segregate land from water is to use bathymetry and elevation information. 30-arc-second resolution of global topography and bathymetry map from SRTM 30 is used to prepare a global flag file (Appendix II; Figure 2 a**).** Pixels corresponding to elevation value > 0.0 is denoted or flagged as land pixels. Since backscattering by suspended materials in turbid coastal environment will lead to severe over-estimation of the aerosol contribution leading to over correction of the radiance and low or negative water-leaving radiances at blue –green channels in standard atmospheric correction, pixels corresponding to bathymetry value of < 50 m is symbolized as shallow waters and flagged (Appendix II; Figure 2 b). Rest of the pixels is denoted as clear pixels for processing.

4.3.2 Cloud masking

For discrimination of cloud's presence over open ocean, Rayleigh corrected reflectance threshold is 2.7% in NIR region and less than 2.7% in SWIR (Wang and Shi, 2006). Therefore, the approach of Rayleigh corrected reflectance threshold generation is adopted i.e. ~2.7% at 870 nm for Oceansat-3 OCM over the open ocean. The reflectance greater than or equal to 0.027 at NIR indicates the presence of clouds over there with aerosol optical thickness at 870 nm nearly '0.3'. This method was also adopted for SeaWiFs and Modis (Wang and Shi, 2006). While in the case of coastal region, optically complex water contributes to the top of the atmosphere reflectance in NIR region, thus making it difficult to mask the clouds. The presence of one more channel in SWIR i.e. 1010 nm in OCM-3 is advantageous since water reflectance can be negligible due to strong absorption by water. Since clouds show a spectrally flat signature, reflectance ratio will also be very less as compared to ocean and aerosols.

4.3.3 Sun glint Characterization and masking

OCM-1 and OCM-2 used a payload steering mechanism to tilt the sensor by ± 20 degree so as to reduce the glint affected area and minimize the glint over Indian subcontinent. The same strategy is followed in OCM-3. However, due to its fixed orbit geometry, the global coverage of OCM-2 had permanent glint covered areas which shifted according to seasons causing data gaps in

monthly binned images This configuration of OCM-2 made it impossible to study basin scale properties of global oceans for climate related applications. Therefore, in OCM3, a marching orbit was configured to obtain glint free data every 6-7 days. Sun glint is a phenomenon observed in ocean colour images due to the relative orientation of the sun and the ocean colour sensor. For a certain sun-sensor geometry, the surface of the ocean acts as a strong specular reflector reflecting the sun rays back to the sensor. In a typical ocean colour image, the peak of sunglint occurs at the specular image of the Sun. The ocean surface roughened by the winds, breaks the Sun's image into a multitude of smaller pieces distributed around the specular image (Mohan et al. 2001). Thus the incoming radiation is specularly reflected back to the sensor without interacting with water constituents. In ocean color remote sensing, the sensor-measured radiance at the top of the ocean-atmosphere system can be written as

$$L_t(\lambda) = L_r(\lambda) + L_a(\lambda) + L_{ra}(\lambda) + T(\lambda)L_g(\lambda) + t(\lambda)L_{wc}(\lambda) + t(\lambda)L_w(\lambda) \quad (2)$$

Where $L_r(\lambda)$, $L_a(\lambda)$, and $L_{ra}(\lambda)$ are the radiance contributions from multiple scattering of air molecules (Rayleigh scattering with no aerosols), aerosols (no molecules), and Rayleigh-aerosol interactions, respectively. $L_g(\lambda)$ is the specular reflection from the direct Sun (sun glint) radiance, $L_{wc}(\lambda)$ is the radiance at the sea surface resulting from sunlight and sky-light reflecting off whitecaps on the surface, and $L_w(\lambda)$ is the water leaving radiance. $T(\lambda)$ and $t(\lambda)$ are the atmospheric-direct and diffuse transmittances in the sensor-viewing direction respectively. The sun glint radiance can be written as:

$$L_g(\lambda) = F_0(\lambda)T_0(\lambda)L_{GN} \quad (3)$$

Where $F_0(\lambda)$ and $T_0(\lambda)$ are the extraterrestrial solar irradiance (adjusted for the Earth-Sun distance variations) and the atmospheric direct transmittance at the solar direction, respectively. L_{GN} is the normalized sun glint radiance. For a given ocean color image pixel, the value of L_{GN} depends on the solar and the viewing geometry, the sea-surface wind speed and the wind direction. The normalized glint radiance is calculated as follows:

$$L_{GN} = \frac{\rho(\omega) * p(\theta_s, \phi_s, \theta_v, \phi_v, W)}{4\pi * cos^4\beta * cos\theta_v * cos\theta_s} \quad (4)$$

$p(\theta_s, \phi_s, \theta_v, \phi_v, W)$ is the probability density function of sea surface slope dependent on solar zenith angle (θ_s), solar azimuth angle (ϕ_s), sensor zenith angle (θ_v), sensor azimuth angle(ϕ_v) and wind (W) given as

$$p(\theta_s, \phi_s, \theta_v, \phi_v, W) = \frac{1}{2\pi * \sigma_c * \sigma_w} * \exp(-\frac{(\xi^2+\eta^2}{2}) \quad (5)$$

Where $\xi = z_x/\sigma_w$, $\eta = z_y/\sigma_c$ are normalized surface slopes, σ_w and σ_c are the root mean square slopes in the downwind (x) and crosswind (y) directions. In this equation x is taken as the downwind direction. z_x and z_y are the downwind and crosswind components of the facet slopes given by Susan et al (2009)

$$z_x = -\frac{sin\theta_s * cos\Phi_s + sin\theta_v * cos\Phi_v}{cos\theta_s + cos\theta_v} \quad (6)$$

$$z_y = -\frac{sin\theta_s * sin\Phi_s + sin\theta_v * sin\Phi_v}{cos\theta_s + cos\theta_v} \quad (7)$$

There are various techniques of estimating σ_w and σ_c. SeaWiFS (Sea-viewing Wide Field-of-view Sensor) used a simplified version of σ_w and σ_c neglecting the effect of wind direction. The mean square slopes used by SeaWiFS s are given below.

$$\sigma_w \cong \sigma_c \cong mss = 0.0493W^{0.5} \quad (8)$$

MERIS (Medium Resolution Imaging Spectrometer) uses the following values of mean square slopes.

$$\sigma_w = 0.00316 * W^{0.5} \quad (9)$$

$$\sigma_c = (0.003 + 0.00192 * W)^{0.5} \quad (10)$$

Where W is the wind speed in m/s.

β is the angle between the facet normal and the normal to the local surface given by

$$\beta = cos^{-1}[\frac{(\cos\theta_s + cos\theta_v)}{2cos\omega}] \quad (11)$$

Where θ_s is the solar zenith angle, θ_v is the sensor zenith angle and ω is the angle of incidence.

$\rho(\omega)$ is the Fresnel reflectance given as

$$\rho(\omega) = 0.5 * [(\frac{\sin(\omega-\omega')}{\sin(\omega+\omega')})^2 + (\frac{\tan(\omega-\omega')}{\tan(\omega+\omega')})^2] \quad (12)$$

Where ω is the angle of incidence and ω' is the angle of refraction, ie, sin(ω')=sin(ω)/n. The refractive index n is taken as 4/3 regardless of wavelength.

The normalized glint radiance is calculated for all pixels of OCM3 and pixels with L_{GN} >0.005 are masked based on Wang and Bailey 2001 method. The residual sun glint will be corrected using a sun glint correction algorithm which will be implemented on OCM3 global data on a pilot basis. Cross Calibrated Multiplatform (CCMP) derived surface wind velocity (0.25°X0.25°) datasets are used for sun glint characterization and residual glint removal. The details are given in Appendix I

4.3.4 Atmospheric correction

In ocean colour remote sensing, radiance at the sensor level can be modeled using molecular scattering and particle scattering based on existing mathematical models and gaseous absorption in the atmosphere, provided solar and satellite viewing geometry are known. Path radiance due to Rayleigh scattering (L_r) computed for single scattering approximation can be expressed as given in *(Gordon et al. 1988).* The total signal received at the sensor level is the linear combination of atmosphere through scattering and absorption processes and transmittance of water leaving radiance from surface to sensor level. Basis of the algorithm for removing the atmospheric effects from satellite data over water bodies is to derive normalized water-leaving radiance/ remote sensing reflectance in the visible range. Atmospheric path radiance arises due to scattering effects of atmospheric gases and aerosols. Scattering of electromagnetic radiation by atmospheric gaseous molecules, known as Rayleigh scattering, occurs when light is elastically scattered by particles which are much smaller than the wavelength of light. Radiance resulting from Rayleigh scattering can be calculated using existing mathematical models, provided solar and satellite viewing geometry are known. The model also requires atmospheric pressure to adjust the value of Rayleigh optical thickness. Aerosols on other hand, are particles (liquid or solid) suspended in atmosphere which are much larger than the gas molecules. Optical properties of aerosol depend mainly upon their particle size distribution and refractive index. Radiative transfer model equations are given as equations from 13-26 in Table -5

13) $L_w = {}_nL_w \cdot \cos(\theta_s).\exp[-(0.5\tau_{r+}\ \tau_{oz}).(1/\cos(\theta_s))]$

14) ${}_n\rho_w = \pi.nL_w/F_0$

15) $\rho_w = {}_n\rho_w \cdot \exp[-(0.5\tau_{r+}\ \tau_{oz}).(1/\cos(\theta_s))]$

16) $\rho_w = {}_n\rho_w.t_u(\theta_s, \lambda)$

17) $F'_o(\lambda) = F_o(\lambda)\ \exp[-\tau_{oz}(1/\cos(\theta_v) + 1/\cos(\theta_s))]$

18) $L_r = \tau_r(\lambda)\ F'_o(\lambda)\ p_r(\theta_s,\theta_v,\lambda)/(4\pi\ \cos(\theta_v))$

19) $p_r(\theta_s,\theta_v,\lambda) = [P_r(\gamma-,\lambda)+[r(\theta_v)+r(\theta_s)]\ P_r(\gamma+,\lambda)]/\cos(\theta_v)$,

20) $\cos(\gamma\pm) = \pm\cos(\theta_s)\ \cos(\theta_v) - \sin(\theta_s)\ \sin(\theta_v)\ \cos\ (\phi_v - \phi_s)$

21) $P_r(\gamma) = (3/4).[1 + \cos^2(\gamma)]$

22) $\tau_a(\lambda) = A\ (\lambda)^{-\alpha}$

23) $L_a(\lambda) = F'_o(\lambda).\tau_a(\lambda).\omega_a.p_a/(4\ \pi\ .\ \cos(\theta_v))$

24) $T_a = \exp[-\ (\tau_{r+}\tau_{oz+}\tau_a).(1/\cos(\theta_v) + 1/\cos(\theta_s))]$

25) $\epsilon(\lambda_l, \lambda_u) = \rho_{as}(\lambda_l)/\ \rho_{as}(\lambda_u) = \tau_a(\lambda_l).\omega_a(\lambda_l).P_a(\lambda_l)/\ \tau_a(\lambda_u).\omega_a(\lambda_u).P_a(\lambda_u)$

26) $\rho_{path}(\lambda_j) = \rho_r(\lambda_j)\ + \epsilon(\lambda_j, \lambda_u).\ \rho_{as}(\lambda_u)$

Table 5: Radiative Transfer Model Equations

where θ_s and θ_v are solar and viewing zenith angle respectively, whereas ϕ_s and ϕ_v are solar and viewing azimuth angle respectively. $r(\theta)$ is the Fresnel reflectance at the air-water boundary for a light incident at an angle θ. $\tau_r(\lambda)$ is the Rayleigh scattering optical depth and $p_r(\gamma)$ is the Rayleigh scattering phase function. $F'_o(\lambda)$ is the extraterrestrial solar irradiance ($F_o(\lambda)$) corrected for its absorption at the ozone layer.

Different types of aerosols, indicating the aerosol optical depth T_a to be wavelength dependent can be modelled by power law. Where, α is Angstrom exponent and A is constant. Gordon and Wang in 1994 used the Shettle and Fenn, 1979 aerosol model to retrieve the aerosol optical thickness τ_a using two NIR bands. In the case of Oceansat-3 OCM, there are two possibilities, first one, 780 and 870nm bands is used for correcting atmosphere over open ocean. In this way, aerosol from data itself can be retrieved on a pixel to pixel basis. Atmospheric transmittance T_a (Sun to sea surface to sensor) can be estimated using equation (24). Radiance measured L_t at the sensor level is nothing but the linear combination of atmospheric path radiance and diffuse transmittance of radiation to the top of atmosphere t_u times water leaving radiance L_w, and is be expressed as in equation 1 where, L_a and L_r represents radiance reaching the sensor due to aerosol and Rayleigh scattering, respectively. By using equations (2) to (26) in (1), spectral water leaving radiance is retrieved over sea surface.

4.3.4.1 Single scattering approximation

In general, atmospheric path radiance is nothing but the linear combination of three non-linear terms from equation (15) i.e. scattering due to air molecules known as Rayleigh scattering, scattering due to aerosols known as Mie scattering and scattering due to molecules and aerosols both [Deschamps et al., 1983]. The last term accounts the interaction between air molecules and particle scattering. Basically, this term may be a good indicator for the single scattering case i.e. in the case of single scattering, this will become negligible and can be avoided.

4.3.4.2 Aerosol models

Gordon and Wang in 1994 used the aerosol models (Shettle and Fenn 1979) based on different particle size and relative humidity, which resulted in the corresponding change in their refractive indices. The particle size distribution is explained by bimodal log normal distribution. Since

particle size increases with increasing relative humidity(RH) from 0 to 99%. Three type of interpretations can be made based on the particle distribution, one is Aiken or nucleation mode, second one is accumulation mode and third one is coarser mode. Further, under a broader category of aerosols,-two types of aerosols commonly occur in nature. Tropospheric aerosols based on its physical characteristics, fine in nature and oceanic aerosols larger in nature. These two types of aerosols in variable proportion, take the form of some other aerosol categories namely maritime and coastal. Again, tropospheric aerosol consolidates the particle size fraction in the ratio of 7:3 i.e. (70% water soluble and 30% dust like particles) without oceanic contribution. This means the mode radii of tropospheric aerosols is always less than 0.1 um with single scattering albedo from 0.959 to 0.989 and for RH ranging from 0 to 98%. While for the larger fraction as a sea salt component in the oceanic aerosol type, the mode radii is greater than 0.3um as relative humidity (RH) increases from 0 to 98% with single scattering albedo considered to be unity [Gordon, 1997]. Therefore, $\boldsymbol{\epsilon}(\lambda_l, \lambda_u)$ ceases the spectral variation due to swelling in particle size with increasing relative humidity. The next category with the 99% particles of tropospheric nature and 1% oceanic pertains to the category of Maritime aerosol. Similarly, the coastal aerosol model comprises 99.5% tropospheric and 0.5% oceanic.

Using equations 25 and 26, spectral path radiance of the atmosphere is further deduced. Epsilon $\boldsymbol{\epsilon}(\lambda_l, \lambda_u)$,the ratio of aerosol reflectance at 780nm and 870nm over open ocean ise used for generating aerosol models. This model gets further utilized for generation of water leaving radiance/ remote sensing reflectance with aerosol optical thickness at 870nm.

4.3.5 Bio-optical algorithms for EOS-06(OCM)

4.3.5.1 Chlorophyll-a algorithm

For the development of ocean-colour chlorophyll-a algorithm a large number of simultaneous measurements of in-situ radiance/reflectance and chlorophyll-a data preferably coinciding with satellite data (Gordon *et al*., 1983; Balch *et al*., 1992) are required. Using the in-situ data collected from regional and global oceans, chlorophyll-a algorithms were developed for SeaWiFS sensor using semi-analytical, semi-empirical and empirical approaches (O'Reilly *et al*., 1998,2000). A large number of semi-analytical and empirical bio-optical algorithms were evaluated for the in-situ data collected during ship campaigns in the Arabian Sea (Chauhan *et al.,* 2002) among which

OC2 performed well for the estimation of chlorophyll-a. Thus, OC2 algorithm was implemented for routine processing of the ocean colour satellite images of Oceansat-1 OCM data. Further, validation of chlorophyll-a concentrations from satellite images of OCM and in situ measured chlorophyll-a resulted in good agreement having r^2 of 0.90 and RMS error of 0.125 mg m^{-3}. The total validation points were 43 and the range of chlorophyll-a concentration was from 0.072 to 5.9 mg $m^{-3.}$ The OC2 algorithm was developed using the in-situ database called SeaBAM (N=919) (O'Reilly *et al*., 1998).

The NASA bio-optical Marine Algorithm data (NOMAD) set is the largest global, high quality *in-situ* bio-optical data set that is publicly available to develop and validate the satellite ocean-colour algorithms (Werdell and Bailey, 2005). It includes a wide range of chlorophyll-a concentrations from 0.1 to 81.86 mg m-^{3} encompassing a variety of mesotrophic and eutrophic waters. Chlorophyll-a concentrations were acquired using both fluorometric and HPLC methods (Werdell *et al*., 2003). Nearly two-thirds of the chlorophyll-a concentration were measured using HPLC giving better estimations as compared to fluorometric method. Thus all the fluorometrically measured chlorophyll-a values were converted into the HPLC chlorophyll-a concentrations using the following relationship;

$$HPLC\ (Chl) = 0.8105*Fluor\ (Chl) + 0.1931\ (R^2 = 0.9) \quad (27)$$

NASA bio-optical Marine Algorithm data (NOMAD), which comprises of more than 8000 bio-optical measurements along with chlorophyll-a concentration ranging between 0.1 to 81.86 mg m^{-3} (Werdell and Bailey, 2005). The remote sensing reflectance ratios for $R_{rs}443/R_{rs}555$, $R_{rs}490/R_{rs}555$ and $R_{rs}510/R_{rs}555$ were plotted against chlorophyll-a concentration for all the data points. A robust relationship was obtained between maximum band ratio of $R_{rs}443/R_{rs}555$, $R_{rs}490/R_{rs}555$ and $R_{rs}510/R_{rs}555$ and corresponding chlorophyll-a concentration. The maximum R_{rs} band ratios (MBR) verses chlorophyll-a concentration demonstrated a sigmoidal relationship as observed by many researchers (Morel and Maritorena, 2001). A cubic polynomial type functional form was found to best fit the maximum band ratios (MBR) and chlorophyll-a concentration. The cubic polynomial formula yielded good results when tuned with log-transformed merged data set, with a R^2 = 0.8 and RMSE ~ 0.2. Cubic polynomial equation between log transformed chlorophyll and MBR is given as

$$Log_{10}(C) = a+b*R+c*R^2+d*R^3 \quad (28)$$

Where, C represents the chlorophyll-a concentration, R represents the logarithm of MBR of $R_{rs}443/R_{rs}555$, $R_{rs}490/R_{rs}555$ and $R_{rs}510/R_{rs}555$ and a, b, c, d and e are the regression coefficients as listen in Table 6. The developed cubic polynomial equation captures the inherent relationship between the in-situ reflectance band ratios and the chlorophyll-a concentration. The initial algorithm is implemented for Oceansat-3 OCM. Further refinement of the coefficients will be carried out as more data is populated.

Model	Input Band Ratio	Coefficients
$\log_{10}(C)=a+b*R+c*R^2+d*R^3$	R = log10(max[Rrs443, Rrs490, Rrs510]/Rrs555)	a=0.2604; b= -2.8025; c= 3.6626; d= -1.976

Table 6: Regression coefficients for the OCEANSAT-3 chlorophyll-a concentration, algorithm developed using the NOMAD data set.

4.3.5.2 Vertical diffuse attenuation coefficient (K_d) algorithm

The vertical diffuse attenuation coefficient of oceanic water can be retrieved from ocean colour satellite data. Oceanic and coastal production of phytoplankton depends largely on light availability. For this purpose, diffuse attenuation coefficient (K_d) plays a significant role, which defines the presence of light versus depth. Ocean waters have been optically classified based on the relation between diffuse attenuation coefficient and the plant pigment content. The above knowledge is useful in understanding the upper ocean warming, that occurs through absorption of solar irradiance (400-800 nm).

An algorithm has been developed to estimate K_d (490 nm) as a function of ratio of water leaving radiance in 490 nm and 555 nm using the NOMAD merged data set. A cubic polynomial fit was found to best explain the functional relationship between the K_d (490 nm) and ratio of remote sensing reflectance i.e. $R_{rs}(490)/R_{rs}(555)$. Following equation was obtained for the estimation of

K_d (490 nm) using NASA bio optical marine algorithm datasets(NOMAD) with root mean square error of 0.09 and r^2 of 0.92 for log transformed data.

$$Log_{10}(K_d\ 490) = a + b*K + c*K^2 + d*K^3 \quad (29)$$

Where, $K = \log_{10}[R_{rs}(490)/R_{rs}(555)]$ and a= -0.7732; b= -1.6961; c=1.141; d= -0.6511.

The initial algorithm is implemented for Oceansat-3 OCM. Further refinement of the coefficients will be carried out as more data is populated.

4.3.5.3 Total Suspended Matter (TSM) Algorithm

The transport and distribution of suspended sediments in coastal environment is driven by processes such as tides and waves, river discharge, wind stress and turbidity currents. Satellite based remote sensing have proven to be an effective tool for the detection and quantification of total suspended matter in coastal seas (Klemas *et al*. 1974, Tassan and Sturm 1986, Chauhan *et al*. 1996). Suspended sediments also affect the penetration of light, the transport of nutrients and shoreline morphology, among other processes. Several sediment algorithms were proposed to quantify total suspended matter (Tassan and Sturm 1986, Chauhan *et al*. 1997). Based on the approach proposed by Tassan (1994), a TSM algorithm was developed for the operational use with OCEANSAT-1 OCM (Chauhan *et al*., 2003). This algorithm was reported for moderately turbid waters (Surendran *et al*., 2006), which was later modified by Pradhan *et al.* (2005) for highly turbid waters of Hooghly estuary. The modified algorithm was found to be overestimating TSM values in the open ocean waters. OCEANSAT-2 OCM sensor had a new wavelength at 620 nm added for the better quantification of the TSM concentration in the coastal waters. 625 nm wavelength was suggested to be the best for the estimation of TSM concentration in coastal waters (Ahn *et al*., 2001).

A three-component model of ocean colour reflectance proposed by Sathyendranath et al. (1989) was used to simulate a large set of remote sensing reflectance values by independently varying the concentration of chlorophyll-a, suspended matter and yellow substance over the concentration range generally encountered in coastal waters. The simulated data set was subsequently used to construct the estimation of algorithm for TSM in presence of uncorrelated phytoplankton and yellow substance. Using the three-component ocean colour model, a synthetic data set was generated consisting of 1000 reflectance spectra for randomly varying

TSM (S), chlorophyll (C) and yellow substance (Y) concentration. To simulate the range of conditions encountered in coastal waters of the Arabian Sea a random number generator was used to provide model input (C, S, Y) assuming a lognormal distribution of these parameters. All the three variables were assumed to be totally uncorrelated to each other, which is typical of coastal water environment. The input ranges for suspended matter was taken between 1.0 to 250 mg L^{-1}, for chlorophyll-a 0.05 to 5.0 mg m^{-3}, and for coloured organic matter absorption characterized at 440 nm, the range for minimum and maximum variations was fixed between 0.01 to 0.35 m^{-1}. This minimum and maximum ranges for all the three variables were selected on the basis of sea truth data collected in the Arabian Sea. The remote sensing reflectance, R_{rs} and normalized water leaving radiance, L_{wn} were simulated for the first six bands of OCM sensor (i.e. 412, 443, 490, 510, 555, and 620 nm). The relationship between TSM and Rrs620 nm showed more sensitivity for the higher TSM concentration values when compared to 555 nm spectral band. Single band algorithms were developed fitting an exponential relation between modeled reflectance in 555 nm and 620 nm wavelengths and TSM concentration with r^2 of 0.90 for 555 wavelength and r^2 of 0.97 for 620 nm. However, both algorithms were derived using single wavelength therefore they had their own limitation of sensitivity over different ranges of suspended matter concentration. A new algorithm was developed which makes use of the sensitivity to the variability of the absorption and scattering properties of phytoplankton and suspended matter (Tassan 1994). The new algorithm had the form

$$X_s = [R_{rs}(\lambda_{555}) + R_{rs}(\lambda_{620})]*[R_{rs}(\lambda_{555})/R_{rs}(\lambda_{490})] \quad (30)$$

Where X_s is suspended sediment concentration and the first term with $\lambda_{555\ and}\ \lambda_{620}$ is the sensitive term in a zone of low chlorophyll and colored organic matter absorption (essentially because of the high sediment scattering in these wavelengths). The second term with λ_{555} and λ_{490} is the slope zone of the absorption spectra, and thus depending on chlorophyll and colored organic matter absorption at (490), is the compensating term.

A statistical relationship was developed between X_s and TSM concentration and the algorithm yielded by the least square fitting was

$$\text{Log (S)} = 62.80 * X_s + \text{for } 1.0 < S\ (\text{mg } L^{-1}) < 250 \quad (31)$$

This algorithm was found to be more robust compared to a single wavelength relationship using either, $R(\lambda_{555})$ or $R(\lambda_{620})$. Equation (30-31) is used as the operational TSM algorithm with OCM 3

data and if any fine-tuning is needed, it will be done after the initial analysis and validation of the OCM data as more data gets populated.

4.4 Flow Chart/Block Diagram

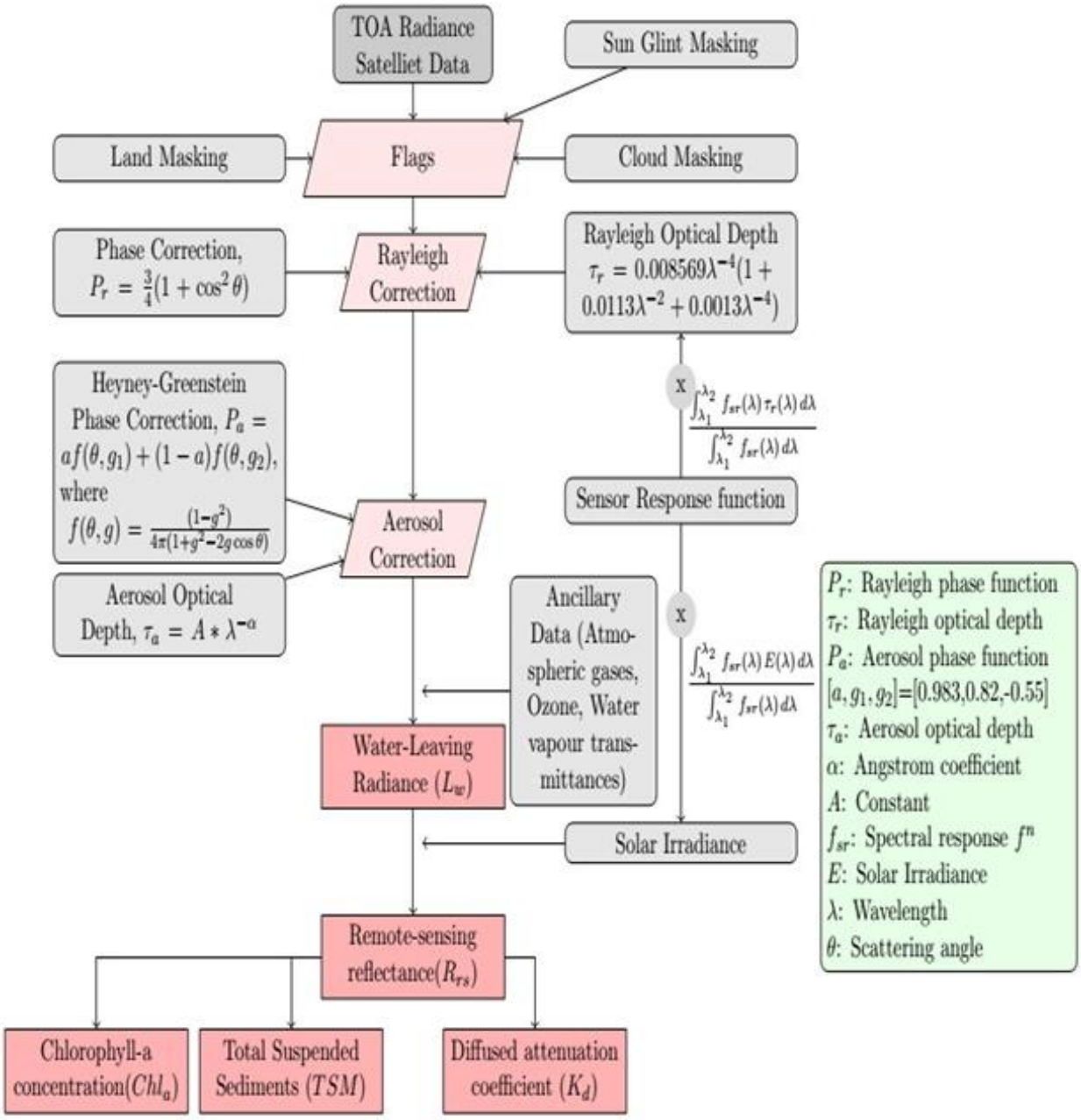

4.5 Masks

Masked pixels are not processed and are typically set to zero so as to eliminate them from future analysis.

mask land	Mask out all land pixels: 0=off
mask cloud	Mask out pixels for which cloud albedo is above user defined threshold: 0=off
mask glint	Mask out pixels with sun glint: 0=off

Table7: Mask description for OCM3

4.6 Error/uncertainty targets of geophysical parameters

The geophysical parameters from OCM-3 and targeted error budget over the variable range (minimum-maximum) is given in Table 8

Sr. No.	Parameter	Variable range	Targeted error budget
1.	Remote sensing reflectance at 412, 443, 490, 510, 555 nm	(0.0-0.1) sr^{-1}	<5%

2.	Chlorophyll *(Chl-a)*	0.05-30.0 mg/m^3	<35%
3.	Vertical diffuse attenuation coefficient(K_d) at 490nm	0.01-0.5 m^{-1}	<15%
4.	Total suspended matter (TSM)	0.0-200.0 $mg\ L^{-1}$	<20%
5.	Aerosol optical depth (AOD) at 870nm	0.0-1.0	<20%

Table 8: Geophysical parameters from OCEANSAT-3 OCM data with targeted error budget

4.6.1 Sensitivity analysis

4.6.1.1 Sensitivity of chl-a retrieval to aerosol spectral optical depth model

In the clear sky condition, the simulation of TOA radiance based on aerosol optical thickness at 870nm (0.1) was carried out. Further change of 5 and 10 % lead in the same proportion to the aerosol radiance, i.e. for 5 to 10% change in aerosol, corresponding change in the following channels is given in Table 9.

aod (% change)	chl-a	Rrs (% change	Rrs (% chang	Rrs (% chang	Rrs (% chang	Rrs (% change
at 870nm	(% change)	in 412nm	in 443nm	in 490nm	in 510nm	in 555nm
5	~1	<0.7	<0.6	<0.7	<0.81	<1.25
10	~2	<1.4	<1.2	<1.3	<1.6	<2.5

Table 9: Percent change in Rrs to change in AOD

4.6.1.2 Sensitivity to changes in atmospheric ozone content

Ozone transmission was simulated using radiative transfer model for clear sky condition i.e. aerosol optical thickness at 550nm 0.2 and ozone thickness 0.4cm-atm and water vapour 1.5

g/cm^2. From 10 to 40% change in ozone, the corresponding change in the ocean colour visible bands is given in Table 10.

oz (% change)	chl-a (% change)	Rrs (% chan in 412nm	Rrs (% cha in 443nm	Rrs (% cha in 490nm	Rrs (% cha in 510nm	Rrs (% cha in 555nm
10	<1	Nil	<0.02	<0.2	<0.3	<0.5
20	<1.5	Nil	<0.04	<0.3	<0.5	<1.0
30	<2.5	Nil	<0.06	<0.5	<0.7	<1.5
40	<3	Nil	<0.08	<0.6	<0.9	<1.8

Table 10. Change in Rrs (412, 443, 490, 510 & 555) due to change in Ozone concentration

4.6.1.3 Sensitivity of AOD retrieval to the aerosol characterization parameters

The aerosol radiances were simulated for aerosol optical thickness at 870nm i.e. 0.01 a very clear sky condition with angstrom exponent -0.016 for oceanic condition. For 5% change in aerosol optical thickness at 870nm, nearly similar changes were observed in the spectral aerosol radiances. The same approach was adopted for different aerosol optical thicknesses i.e. 0.02 and 0.1 respectively to see the corresponding changes in the spectral aerosol radiances as well. The results are given in Appendix-III

5.0 Future scope

5.1 Gap areas in present algorithm

Atmospheric correction procedure is carried out under some constraints 1) the NIR-SWIR bands are assumed to be the dark pixel based on the complete attenuation of light by water bodies while the efficiency of this approach may vary drastically over coastal and open ocean bloom waters 2) for absorbing aerosols, the Gordon and Wang 1994 model may not perform adequately. 3) Maximum band ratio algorithm for chlorophyll concentration will fail over mono specific algal blooms (like Noctiluca spp or Trichodesmium spp).

5.2 Fine-tuning using in-situ data/ special campaign

There will always be some scope time to time for updating the operational algorithms. So to achieve the required outcomes, subsequent field campaigns will be carried out in the initial phase to validate and fine tune the algorithms to achieve the desired accuracy.

6.0 Acknowledgments

The authors express their thank to DD EPSA, PD & APD Oceansat-3 and the review committee for their valuable guidance and suggestions during the review of ATBD.

7.0 References

1. Thuillier, G., M. Hersé, P. C. Simon, D. Labs, H. Mandel, D. Gillotay and T. Foujols, The solar spectral irradiance from 200 to 2400 nm as measured by the SOLSPEC spectrometer from the ATLAS 1-2-3 and EURECA missions, Solar Physics, 214(1): 1-22, 2003.

2. Gao, B.-C., M. J. Montes, R.-R. Li, H. M. Dierssen, and C. O. Davis, An atmospheric correction algorithm for remote sensing of bright coastal waters using MODIS land and ocean channels in the solar spectral region, TGRS, 45, 1835-1843, 2007.

3. Chuanmin Hu, Kendall L. Carder, and Frank E. Muller-Karger, Atmospheric correction of Seawifs Imagery over Turbid coastal waters: A practical method. Remote Sens. Environ. 74:195-206, 2000.

4. H. R. Gordon, "Removal of atmospheric effects from satellite imagery of the oceans," Appl. Opt. 17, 1631–1636 (1978).

5. H. R. Gordon and M. Wang, "Retrieval of water leaving radiance and aerosol optical thickness over the oceans with SeaWiFS: a preliminary algorithm," Appl. Opt. 33, 443–452(1994).

6. Gordon, H. R., Atmospheric correction of ocean color imagery in the Earth Observing system era, J. Geophys. Res., 102, 17081-17106, 1997.

7. H.R. Gordon, J.W. Brown, and R.H. Evans, "Exact Rayleigh scattering calculations for use with the Nimbus 7 coastal zone color scanner", Appl. Opt. 27, 862-871(1988).

8. https://seabass.gsfc.nasa.gov/wiki/NOMAD

9. https://snpp-omps.gesdisc.eosdis.nasa.gov

10. O'Reilly, J.E., Maritorena, S., Mitchell, B.G., Siegal, D.A., Carder, K.L., Graver, S. A., Kahru, M., and McClain, C., Ocean Colour chlorophyll algorithms for SeaWifs, Journal of Geophysical Res., 103, 24937-24953, (1998).

11. O'Reilly, J.E., SeaWifs post launch calibration and validation analyses: Part 3, NASA Tech.Memo. 2000-206892,11 (2000), 49 pp.

12. Shettle, E.P., and Fenn, R.W., Models for the aerosols of the lower atmosphere and the effects

of humidity variationson their optical properties, AFGL-TR-79-0214, 675, 94pp (1979).

13. Tassan, S., and Strum, B., An algorithm for the retrieval of sediment content in turbid coastal waters from CZCS data. International Journal of Remote Sensing, 7, 643-655 (1986).
14. Tassan, S., Local algorithm using SeaWifs data for the retrieval of phytoplankton pigment, suspended sediments and yellow substance in coastal waters, Appl. Opt., vol. 12, pp. 2369-2378, 1994.
15. Werdell, P.J., and Bailly, S.W., An improved in-situ bio-optical dataset for ocean color algorithm development and satellite data product validation. Remote Sensing of Environment, 98(1), 122-140, 2005.
16. Mao, Z., Chen, J., Hao, Z., Pan, D., Tao, B. and Zhu, Q., A new approach to estimate the aerosol scattering ratios for the atmospheric correction of satellite remote sensing data in coastal regions" Remote Sensing of Environment, 132, pp.186-194, 2013.
17. Ruddick, K.G., Ovidio, F. and Rijkeboer, M., Atmospheric correction of SeaWiFS imagery for turbid coastal and inland waters. Applied optics, 39(6), pp.897-912, 2000.
18. Gao, B.C., Montes, M.J., Davis, C.O. and Goetz, A.F., 2009. Atmospheric correction algorithms for hyperspectral remote sensing data of land and ocean. Remote sensing of environment, 113, pp.S17-S24.
19. Gao, B.C., Montes, M.J., Ahmad, Z. and Davis, C.O., 2000. Atmospheric correction algorithm for hyperspectral remote sensing of ocean color from space. Applied optics, 39(6), pp.887-896.

Appendix-I

Sun glint correction algorithms (to be tested and implemented on OCM-3 on a pilot basis).

Figure 1 shows the geometry of sun glint along with the incident and reflected radiation geometry

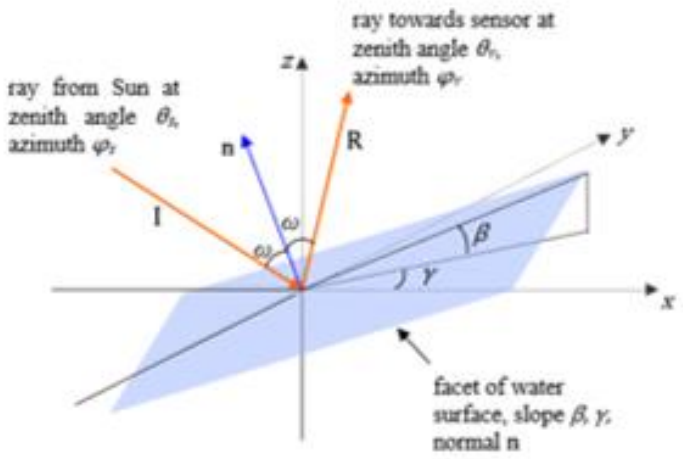

*Figure 1: Sun glint geometry. Light from the sun, travelling along vector I, is reflected by the water surface to the satellite in the direction **R**. The normal to the water surface is **n**. x,y and z form a right-handed axis system, with the z-axis vertically upwards from the mean position of the sea surface. The choice of x-direction is arbitrary-in this paper x is taken as downwind. Zenith angles are measured from the z-axis, azimuth angles clockwise from the x-axis in the x-y plane. The steepest slope of the water surface facet is β, at azimuth γ.*

The sun glint areas will be masked in the operational OCM-3 products based on the normalized glint threshold. However, sun glint correction algorithms will be evaluated on glint contaminated scenes in order to test if geophysical parameters can be retrieved in such areas. Two sun glint correction algorithms are presented

1) The first algorithm is the one used in MERIS (Medium Resolution Imaging Spectrometer). The glint reflectance estimation is performed on every ocean pixels in the data. It uses external knowledge of the wind speed and direction, and the illumination and observation geometry of each pixel to estimate the sun glint contribution to measured reflectance. The estimate of the Sun glint contribution to the ocean signal is based on the Cox and Munk model.

In the visible and NIR the wavelength of light is much shorter than the surface waves, so the incident light can be treated as a ray meeting a flat surface, at an angle ω with the normal **n** to the surface. By laws of reflection, it must be reflected at the same angle and the incident and reflected rays and the normal must lie in the same plane. Therefore, if **I** and R are unit vectors in the direction of the incident and reflected light:

$$R - I = 2cos\omega\, \boldsymbol{n} \tag{12}$$

By setting the components equal on each side of this equation it can be shown that

$$\cos 2\omega = sin\theta_s\, sin\theta_v \cos(\phi_s - \phi_v) + cos\theta_s cos\theta_v \tag{13}$$

$$\cos\beta = \frac{cos\theta_s + cos\theta_v}{2cos\omega} \tag{14}$$

$$\cos\gamma = -\frac{sin\theta_s cos\phi_s + sin\theta_v cos\phi_v}{2cos\omega sin\beta} \tag{15}$$

$$sin\gamma = -\frac{sin\theta_s sin\phi_s + sin\theta_v sin\phi_v}{2cos\omega sin\beta} \tag{16}$$

The facet slope is given by:

$$\frac{\partial z}{\partial x} = z_x = tan\beta cos\gamma \tag{17}$$

$$\frac{\partial z}{\partial y} = z_y = tan\beta sin\gamma \tag{18}$$

Combining equations 17 and 18 with the results of 13 to 16 gives:

$$z_x = -\frac{sin\theta_s cos\phi_s + sin\theta_v cos\phi_v}{cos\theta_s + cos\theta_v} \tag{19}$$

$$z_y = -\frac{sin\theta_s sin\phi_s + sin\theta_v sin\phi_v}{cos\theta_s + cos\theta_v} \tag{20}$$

The probability density function of sea surface slope is given as

$$p(\xi,\eta) = \frac{1}{2\pi * \sigma_c * \sigma_w} * \exp\left(-\frac{(\xi^2+\eta^2}{2}\right)[1 + \ 0.5 * c12 * \xi(1-\eta^2) + \frac{c_{30} * \xi(3-\xi^2)}{6} + \frac{c_{40}(3-6\xi^2+\xi^4}{24} + \frac{c_{22}(1-\eta^2)(1-\xi^2)}{4} + \frac{c_{04}(3-6\eta^2-\eta^4)}{24}] \tag{21}$$

Where $\xi=z_x/\sigma_w$, $\eta= z_y/ \sigma_c$ are normalized surface slopes, σ_w and σ_c are the root mean square slopes in the downwind(x) and crosswind directions. In this equation x is taken as the downwind direction.

In Cox and Munk model, the values of the various constants in the modified Gaussian pdf are as given below

$c_{12}= 0.01 – 0.0086U$, $c_{30}= 0.04 -0.033U$, $c_{40}= 0.23$, $c_{22}= 0.12$, $c_{04}= 0.40$

$$\sigma_w = 0.00316 * W^{0.5} \quad (22)$$

$$\sigma_c = (0.003 + 0.00192 * W)^{0.5} \quad (23)$$

The sun glint reflectance is finally estimated as follows:

$$r_g = \frac{\pi\rho(\omega)*p(\xi,\eta)}{4cos\theta_s cos\theta_v cos^4\beta} \quad (24)$$

The sun glint reflectance is then converted into TOA reflectance using an estimate of atmospheric transmittance as follows:

$$t = \exp(-\frac{(\tau_r+\tau_{oz})}{cos\theta_s} * \exp(-\frac{(\tau_r+\tau_{oz})}{cos\theta_v} \quad (25)$$

$$r_g^* = r_g * t \quad (26)$$

2) The second algorithm uses a simplified version of probability density function ignoring the skewness terms and representing the probability density function as a pure Gaussian function.

The simplified probability density function is given as

$$p(\xi,\eta) = \frac{1}{2\pi*\sigma_c*\sigma_w} * \exp(-\frac{(\xi^2+\eta^2}{2}) \quad (27)$$

This algorithm simplifies the mean square slopes and treats the root mean square slopes in downwind and crosswind direction (σ_w and σ_c) as equal. The simplified form is

$$\sigma_w \cong \sigma_c \cong mss = 0.0493W^{0.5} \quad (28)$$

The sun glint reflectance is then estimated using equation 25 with the simplified $p(\xi,\eta)$.

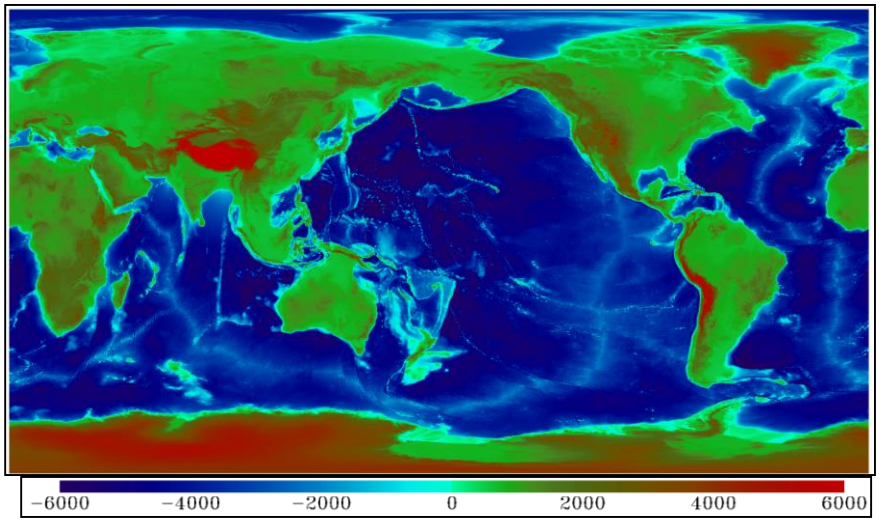

Figure 2 a): Bathymetry and elevation map

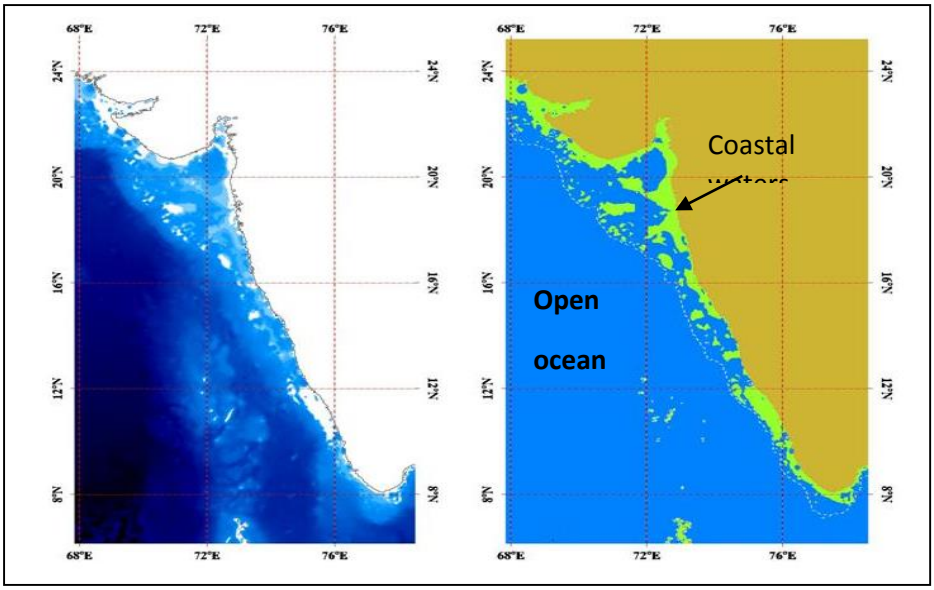

Figure 2 b): Flag image generated for shallow and coastal pixels (green colour) less than 50m depth.

Appendix-III

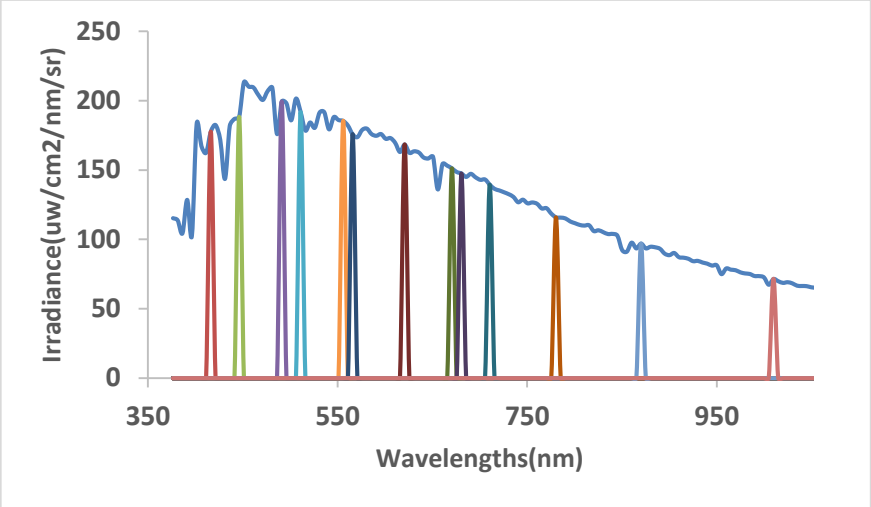

Figure 3: Spectral bands of the OCM-3 sensor.

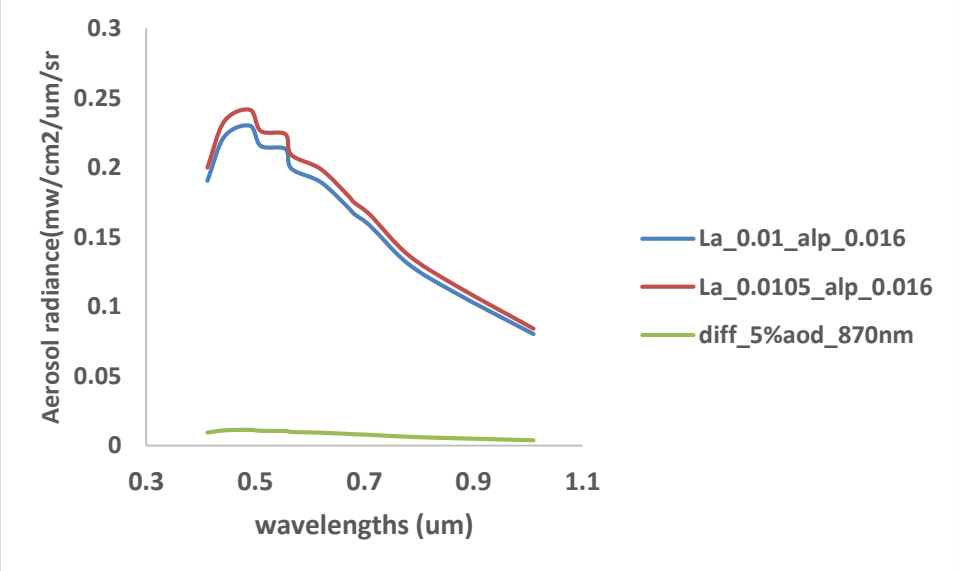

Figure 4: The spectral aerosol radiance simulation for 5% change in aerosol ($\tau_{870} = 0.01$ and $\alpha = -0.016$).

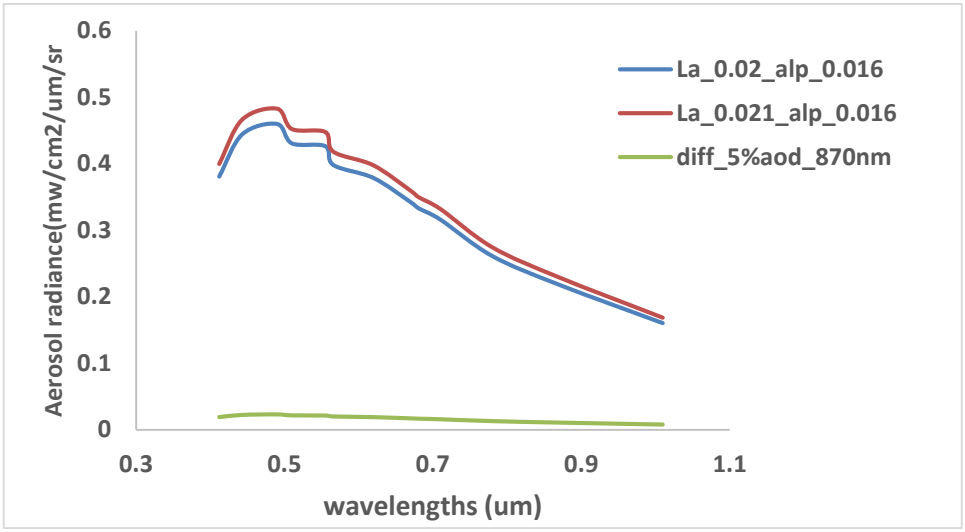

Figure 5: The spectral aerosol radiance simulation for 5% change in aerosol($\tau_{870} = 0.02$ and $\alpha = -0.016$).

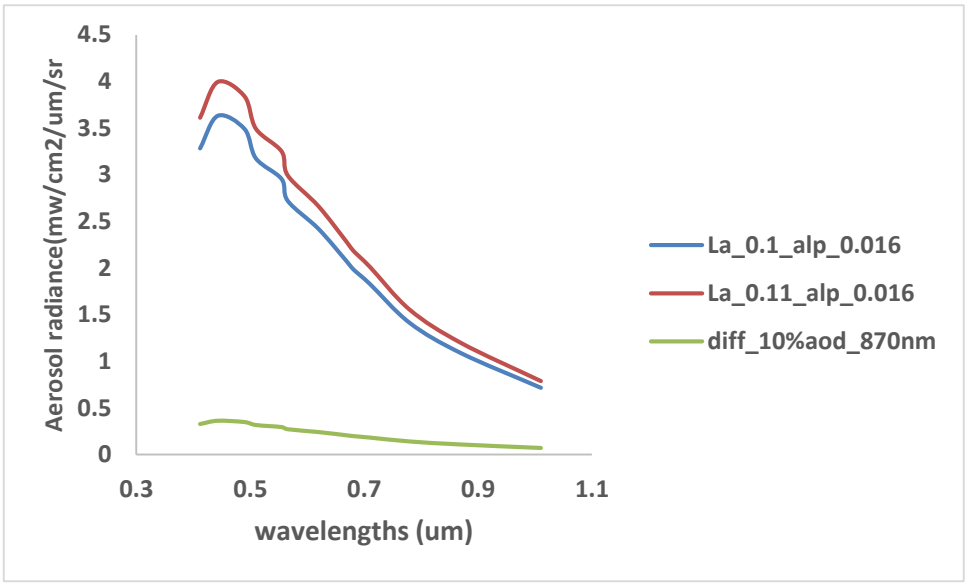

Figure 6: The spectral aerosol radiance simulation for 10% change in aerosol ($\tau_{870} = 0.1$ and $\alpha = -0.016$).

The figure 4 shows that for 5% change in aerosol optical thickness at 870nm, nearly similar changes were observed in the spectral aerosol radiances. Similarly, in figure 5 and figure 6, the same approach was adopted for different aerosol optical thicknesses i.e. 0.02 and 0.1 respectively to see the corresponding changes in the spectral aerosol radiances as well.